



**HAL**  
open science

## Optimal design of a Thermodynamic Vent System for cryogenic propellant storage

Samuel Mer, David Fernández, Jean-Paul Thibault, Christophe Eric Corre

► **To cite this version:**

Samuel Mer, David Fernández, Jean-Paul Thibault, Christophe Eric Corre. Optimal design of a Thermodynamic Vent System for cryogenic propellant storage. *Cryogenics*, 2016, 80 (part 1), pp.127-137. 10.1016/j.cryogenics.2016.09.012 . hal-01516088

**HAL Id: hal-01516088**

**<https://hal.science/hal-01516088>**

Submitted on 28 Nov 2022

**HAL** is a multi-disciplinary open access archive for the deposit and dissemination of scientific research documents, whether they are published or not. The documents may come from teaching and research institutions in France or abroad, or from public or private research centers.

L'archive ouverte pluridisciplinaire **HAL**, est destinée au dépôt et à la diffusion de documents scientifiques de niveau recherche, publiés ou non, émanant des établissements d'enseignement et de recherche français ou étrangers, des laboratoires publics ou privés.

# Optimal Design of a Thermodynamic Vent System for Cryogenic Propellant Storage

Samuel MER<sup>a,b</sup>, David FERNANDEZ<sup>a,b</sup>, Jean-Paul THIBAUT<sup>a,b</sup>, Christophe CORRE<sup>c</sup>

<sup>a</sup>Univ. Grenoble Alpes - LEGI, 38041 Grenoble Cedex 9, FRANCE

<sup>b</sup>CNRS - LEGI, 38041 Grenoble Cedex 9, FRANCE

<sup>c</sup>Ecole Centrale de Lyon - LMFA, 69134 Ecully Cedex, FRANCE

## Abstract

Future operations in space exploration require to store cryogenic liquids for long duration. Residual heat loads, due to heat conduction in the launcher structure or solar radiation, induce cryogenic propellant vaporization and tank self-pressurization. The Thermodynamic Vent System (TVS) permits to control self-pressurization using the following procedure : a fraction of liquid propellant is removed from the tank by a pump, cooled down by a heat exchanger and re-injected inside the tank as a jet or a spray. As no natural heat sink is available in space, the cold source is created by removing another fraction of liquid propellant which is expanded in a Joule-Thomson valve and vented to space. The sub-cooled injection is followed by vapor condensation and liquid bath destratification due to mixing. In this work, an optimization method is applied to an extended homogeneous thermodynamic model to design a TVS system maximizing the storage duration under various heat load and tank size assumptions.

**Keywords:** Long Duration space Mission, Cryogenic Propellant Storage, Thermodynamic Vent System, Performance Optimization

## 1. Introduction

Refueling with cryogenic propellants in Earth orbit is an option currently considered to send rockets on deep space missions since it provides a significant increase of the delivered payload mass (1). The ability to transfer liquid in a micro-gravity environment must be however demonstrated and the capacity to store cryogenics for a long duration remains a key issue (2). The present work is precisely focused on this second technological barrier. Residual heat loads, due to heat conduction in the launcher structure or residual solar fluxes, induce cryogenic propellant vaporization and tank self-pressurization. Due to the extended duration of the mission, an un-controlled tank self-pressurization is bound to lead to storage failure.

The first technical solution to tackle this issue is the implementation of a relief valve (see Fig.1). This type of pressure control system is known as Direct Venting (hereafter denoted DV) (3). The main advantages of DV are its straightforward implementation and sizing. As

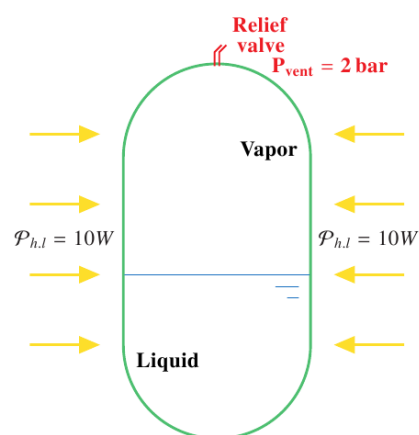


Figure 1: Schematic view of a  $LH_2$  tank submitted to a 10 W heat load and regulated thanks to a relief valve triggered at 2 bar.

can be observed in Fig.2, the tank pressure level remains constant during a DV regulation and is fixed by the relief valve venting pressure. Considering ideally a perfect DV system which vents only pure vapor cryogen, the expelled vapor flow rate is adjusted, depending on the

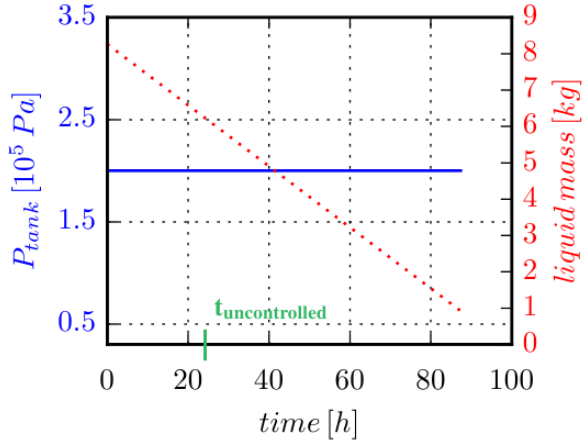


Figure 2: Pressure (blue) and liquid mass (red) evolution in 137 L tank initially filled at 90% during a DV pressure regulation. The uncontrolled tank life expectancy is specified by the green dash.

heat load induced liquid evaporation, to maintain a constant tank pressure. Consequently, the cryogenic liquid mass linearly decreases, from an initial 90% liquid filling (*initial condition of all runs presented in this study*), until the tank is emptied. From now on, a so-called empty tank will actually correspond to the state where the liquid volume in the tank goes below 10% of the tank volume. This state is achieved after roughly 90 h for a 137 L tank. Fig.2 also displays (see green dash) the life expectancy of the same tank without any pressure control : after 23 h only, the tank pressure reaches its maximum allowable value ( $p_{max} = 3.5 \times 10^5 Pa$ ). In this example, DV regulation thus permits to multiply the tank life expectancy by a factor close to four. Unfortunately, in micro gravity, the liquid phase distribution in the tank is such that it is likely DV will lead to venting out cryogenics as a liquid phase. Liquid venting drastically increases the tank emptying speed as observed in Fig.3 where the time  $t_{DV}$  needed to empty the tank is plotted as a function of the prescribed venting pressure, for various liquid mass fraction  $\theta$  of the expelled propellant -  $\theta = 0\%$  corresponds to the previously considered ideal (pure vapor) DV. One can observe in Fig.3 that the performance of an ideal DV system ( $\theta = 0\%$  curve) increases when the venting pressure decreases. This behavior is due to the fact that the density ratio  $\frac{\rho_{liq}}{\rho_{vap}}$  between the liquid hydrogen and its vapor increases when the pressure decreases. When the liquid mass fraction of the vented fluid is no longer zero, the venting time dramatically decreases (see  $\theta = 5\%$  or  $25\%$  in Fig.3). Since no device ensures pure vapor removal from the

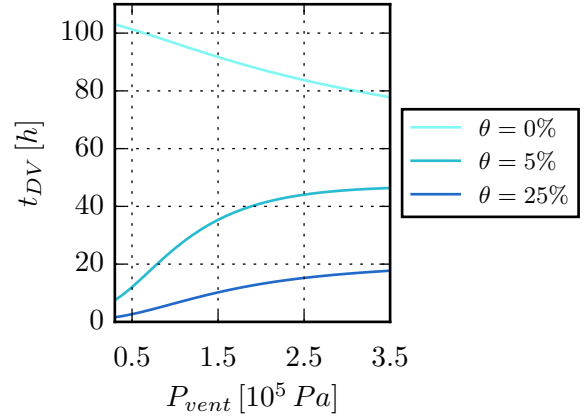


Figure 3: Influence of the relief valve venting pressure ( $p_{vent}$ ) and the liquid mass fraction of the expelled propellant ( $\theta$ ) on the DV venting time for a 137 L tank submitted to 10 W heat load.

tank in micro-gravity environment, the DV regulation system appears inappropriate to manage tank pressure for long-duration space missions. However the venting time computed for an ideal DV system provides a target performance (depending on tank volume, heat load and operating pressure) for an alternative regulation strategy designed to operate in space conditions.

Such a pressure regulation system adapted to micro-gravity space condition has been developed at NASA in the nineties and is called Thermodynamic Vent System (see (4) (5) (6) (7)). The TVS control strategy is based on the following process : a fraction of liquid propellant is removed from the tank by a pump, cooled down by a heat exchanger and re-injected inside the tank as a jet or a spray (see Fig.4). As no natural heat sink is available in space, the cold source is created thanks to the vented branch. The subcooled injection is followed by vapor condensation and liquid bath destratification due to mixing resulting in a tank pressure reduction.

Recently, Barsi (8) (9) (10) and Demeure (11) have studied TVS control systems using on-ground small scale experiments with simulant fluids. These works evidenced some difficulties that need to be overcome for properly managing the thermal boundary condition at the tank wall for on-ground laboratory experiments. This issue was recently tackled in (12) using an active wall insulation technique. Despite non-ideal adiabatic conditions, Barsi and Demeure were both able to demonstrate that measured trends for tank pressure and temperature could be correctly predicted with an homogeneous thermodynamic model. Such a model describes the physical phenomena occurring in the tank

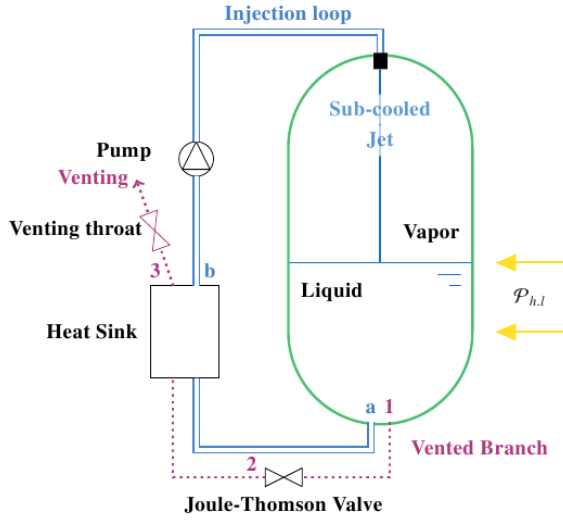


Figure 4: Schematic view of a TVS controlled tank. The (blue) injection loop drives directly a subcooled jet inside the ullage. The (violet) vented branch creates the cold source heat sink.

during self-pressurization and TVS injection from thermodynamic balance equations. Liquid and vapor phases are assumed to remain in thermal equilibrium during the regulation history. It is further assumed that both phases remain at the saturation temperature corresponding to the tank ullage pressure. This model yields an accurate prediction of tank temperature and pressure evolution during self-pressurization and TVS regulation when compared with available on-ground experiments (see (13) and subsection 3.4 of the present paper). However, the model does not take explicitly into account gravity effects as it relies on global balance equations inside the tank. Experimental data being currently unavailable for space conditions, the future validation of the model for low or zero gravity conditions will rely on high-fidelity numerical simulations, still in development at this stage (see for instance (14)).

In 2012, the Cryogenic Propellant Storage & Transfer (CPST) demonstration mission program was initiated by NASA (15) (16). One of the main objectives of this mission is to demonstrate on a low-earth orbit flight that cryogenics can be stored in such a way their availability for use is maximized regardless of the mission duration. A demonstration of TVS is also scheduled in this framework in a tank of 137 L submitted to a 10 W heat load.

The objective of the present study is to design such a TVS system, described in detail in Sec.2, so as to maximize its efficiency, *i.e.* its ability to extend the storage life of  $LH_2$ , for various heat load and tank size as-

sumptions. To this end, a numerical model of the whole control system is developed in Sec.3. The homogeneous thermodynamic model governing equations, developed in (11) (in French) and in (13), are briefly presented and extended by adding a description of the various system components (Joule-Thomson valve, heat exchanger, venting throat, pump). Details of the complete system components formulation are provided in Appendix A. A typical model regulation history is presented in Sec.4 for an arbitrarily designed (thus not optimized) TVS system. The optimal design problem is formulated as a multi-parameter and multi-objective optimization problem in Sec.5 and solved using a global (genetic algorithm) optimization method. The sets of optimal solutions are analyzed in Sec.6, first for the CPST mission case and next for different tank size and heat load assumptions, in order to identify some general guidelines for the design of an efficient TVS system.

## 2. Overview of a TVS system

A  $LH_2$  storage tank of volume 137 L is submitted to a prescribed thermal heat load, equal to 10 W and assumed to remain constant throughout the control process. A typical TVS regulation sequence is a succession of cooling phases, where a subcooled jet decreases the tank pressure down to a prescribed minimum value, and self-pressurization phases, where the subcooled jet is turned off and the tank self-pressurizes due to the external heat load, up to a prescribed maximum value  $p_{max}$ . A TVS system is composed of two main branches (see Fig.4) : the injection loop, where the liquid is sub-cooled before entering back in the tank with a prescribed mass flow rate and the vented branch, which permits to create the exchanger cold source thanks to a Joule-Thomson valve and a venting critical throat. The entire TVS system planned for the CPST mission includes the aforementioned components plus the heat exchanger and the circulation pump for the re-injected subcooled liquid, all of which must be contained inside the tank. The following section reviews the design parameters involved in both the vented branch and the injection loop.

### 2.1. Vented branch

While the vented branch is turned on, the thermodynamic system is open to the outer space where the pressure is null. A critical venting throat, characterized by its section radius  $R_{vent}$ , expels the flow into space and limits the mass flowrate  $\dot{m}_{TVS}$  to a critical value depending on the tank inside pressure. The TVS system regulation pressure is characterized by :  $p_{max}$ , the maximum

pressure allowed in the tank (*i.e.*  $\max(p_1)$  in Fig.5) and  $p_{min}$ , the minimum pressure allowed downstream the JT valve (*i.e.*  $\min(p_2)$  in Fig.5). The vented branch also

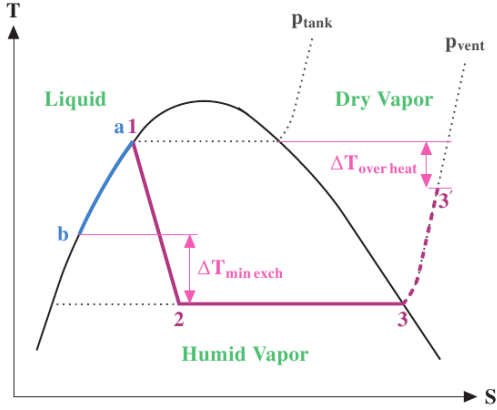


Figure 5: Description of the TVS system in the  $T - S$  diagram. The Vented branch (violet) full line represent the thermodynamic cycle when overheating is forbidden in the heat exchanger ( $\alpha_{OH} = 0$ ). The dashed line from 3 to 3' correspond to the vented vapor overheating when  $\alpha_{OH} = 1$ .

creates the heat exchanger cold source. As is customary when dealing with cryogenes, the cooling function is ensured by a Joule-Thomson valve (see isenthalpic transformation  $1 \rightarrow 2$  on the T-S diagram in Fig.5), that is a section restriction lowering the flow pressure and temperature. The valve is characterized by a pressure drop constant  $K_{JT}$  (17).

## 2.2. Injection Loop

The injection loop function is to withdraw a liquid fraction from the tank, to cool it down in the heat exchanger (see transformation  $a \rightarrow b$  on the T-S diagram in Fig.5) thanks to the vented branch cooling power (see vaporization  $2 \rightarrow 3$  on the T-S diagram in Fig.5) and to inject it back in the tank thanks to a pump with a prescribed mass flow rate  $\dot{m}_{inj}$ .

The heat exchanger uses the plate heat exchanger technology for compactness reason. Its dimensions are the plates length, width, thickness and the flow gap thickness between two plates, respectively :  $L_{plate}$ ,  $l_{plate}$ ,  $t_{plate}$ ,  $\beta_{plate}$ . Since the heat exchanger inlet conditions are continuously varying during a cooling phase, the fixed number of plates  $n_{plate}$  used to design the heat exchanger is necessarily a trade-off between the various operating conditions. This trade-off is described by a coefficient  $\alpha_{exch}$  which sets the plate number between the two extreme values corresponding to the pressure

limits of the control cycle ( $p_{max}$  and  $p_{min}$ ). The  $\alpha_{OH}$  parameter defines the type of heat exchange considered in the heat exchanger on the vented branch side. If  $\alpha_{OH} = 0$ , the sole evaporation cools the injection loop down (see transformation  $2 \rightarrow 3$  on Fig.5). If  $\alpha_{OH} = 1$ , once the fluid is fully evaporated, overheating of the vapor is allowed in the heat exchanger (see transformation  $3 \rightarrow 3'$  on Fig.5) to cool more efficiently the injected fluid. Overheating allowance results in a larger heat exchanger which lowers the available space, in the tank, for cryogen. An optimum between heat transfer efficiency and size has thus to be found.

The second component of the injection loop is the circulation pump, whose function is to ensure the sub-cooled liquid is flowing at the prescribed mass flowrate  $\dot{m}_{inj}$ , overcoming the pressure drops in the heat exchanger. The pump hydraulic efficiency is assumed constant and such that  $\eta_{hyd} = 0.5$  following (18). From the thermal point of view, the hydraulic losses are included through additional internal heat load.

## 3. TVS modelling algorithm

The algorithm developed here to model the TVS system under study takes into account 12 input parameters. Five of these characterize the injection loop : the heat exchanger plates dimensions  $L_{plate}$ ,  $l_{plate}$ ,  $t_{plate}$ ,  $\beta_{plate}$  and the model parameter  $\alpha_{exch}$  allowing to set the plate number depending on the pressure regulation limits. The vented branch is characterized by two parameters : the venting throat radius  $R_{vent}$  and the Joule-Thomson valve constant  $K_{JT}$ . Furthermore the regulation scheme is characterized by five parameters : the pressure limits  $p_{min}$ ,  $p_{max}$  and  $\alpha_p$  which allows to further refine the regulation by linearly decreasing, over the successive control cycles, the maximum pressure initially set to  $p_{max}$ , the injection loop mass flow rate  $\dot{m}_{inj}$  and  $\alpha_{OH}$  which defines whether overheating is applied or not in the heat exchanger (see Fig.5). The TVS modelling algorithm can be decomposed into three phases : the initialization procedure, the cooling phase and the self-pressurization phase, which are successively described. The computation of the tank thermodynamic state by an homogeneous thermodynamic model is detailed in the present section as it is a key original ingredient of the TVS numerical model next applied to TVS optimization. Details on the algebraic relationships used to describe the system components (JT-valve, injection pump, venting throat and heat exchanger) are provided in Appendix A since these descriptions are standard.

### 3.1. Initialization procedure

The first step of the model is to compute the number of plates for the heat exchanger from the assumed plate dimensions, the pressure regulation limits and the parameter  $\alpha_{exch}$ . The plate number for the two most constraining cases (respectively  $p_{min}$  and  $p_{max}$ ) are each computed using the standard Logarithmic Mean Temperature Difference method. The actual fixed size of the heat exchanger is defined with a number of plates computed as a linear combination, with weight  $\alpha_{exch}$ , of the two previous limit designs. Based on the heat exchanger design, the pump power needed to overcome the pressure drops in the heat exchanger is derived. When the pump is turned on, the pump internal heating dissipation  $\mathcal{P}_{pump}^{therm}$  is added to the constant external heat load  $\mathcal{P}_{h.l.}$  to yield a corrected tank heat load ( $\mathcal{P}_{h.l.}^* = \mathcal{P}_{h.l.} + \mathcal{P}_{pump}^{therm}$ ). The initial mass of cryogen is calculated from the initial tank pressure ( $p_{max}$ ) and the initial liquid tank filling assumed equal to 90%. Following this initialization process, a succession of cooling and self-pressurization phases are performed until the liquid mass in the tank reaches a stopping value, corresponding to a 10% liquid filling of the total tank volume considering a pressure of  $1.0 \times 10^5 Pa$ .

### 3.2. Cooling phase

The pressure evolution during an injection phase is predicted using a homogenous thermodynamic model which iterates over successive thermodynamic equilibrium states with a timestep  $\Delta\tau$ . The vapor mass variation  $\Delta m_{vap}^m$  during each timestep is a direct consequence of the competition between the corrected tank heat load  $\mathcal{P}_{h.l.}^*$  and the subcooled jet cooling power  $\mathcal{P}_{jet}$  expressed as :

$$\mathcal{P}_{jet} = \dot{m}_{inj} \cdot c_{liq} \cdot (T_a - T_b) \quad (1)$$

The tank energy balance yields the following expression for the vapor mass variation :

$$\Delta m_{vap}^m = \frac{(\mathcal{P}_{h.l.}^* + \dot{m}_{inj}(c_{liq}(T_{inj}^m)T_{inj}^m - c_{liq}(T_1^m)T_1^m))\Delta\tau}{(c_{vap}(T_1^{m+1})T_1^{m+1} - c_{liq}(T_1^{m+1})T_1^{m+1}) + L_{vap}(T_1^{m+1})} - \frac{\dot{m}_{vap}^m \cdot \Delta(c_{vap} \cdot T) + \dot{m}_{liq}^m \cdot \Delta(c_{liq} \cdot T)}{(c_{vap}(T_1^{m+1})T_1^{m+1} - c_{liq}(T_1^{m+1})T_1^{m+1}) + L_{vap}(T_1^{m+1})} \quad (2)$$

where  $\Delta(c_{vap} \cdot T) = c_{vap}(T_1^{m+1})T_1^{m+1} - c_{vap}(T_1^m)T_1^m$  and similarly for  $\Delta(c_{liq} \cdot T)$ ; moreover, the latent heat of evaporation is assumed to vary linearly with respect to the temperature :

$$L_{vap}(T) = a \cdot T + b \quad (3)$$

where  $a$  and  $b$  depends on the fluid under consideration. Besides, since the model assumes that the fluid remains

at saturation during the regulation process, the Clausius-Clapeyron equation can be integrated to derive a second formulation for the vapor mass variation :

$$\Delta m_{vap}^m = m_{vap}^m \left( 1 - \exp\left(-\frac{Mb}{R} \left(\frac{1}{T_1^{m+1}} - \frac{1}{T_1^m}\right)\right) \right) \times \left(\frac{T_1^{m+1}}{T_1^m}\right)^{\frac{aM}{R}-1} \quad (4)$$

with  $M$  the hydrogen molar mass and  $R$  the universal gas constant.

The non-linear equation satisfied by the new tank temperature  $T_1^{m+1}$  is derived from (2) and (4) and solved at each time step using a Newton method. The cryogen masses (*i.e.* liquid and vapor) are next updated based on  $\dot{m}_{TVS}$  and  $\Delta m_{vap}$ . The model iterates in time until the tank pressure reaches  $p_1^{end}$ , which corresponds to a pressure downstream the JT valve (*i.e.* point 2 in Fig.5) equal to  $p_{min}$ .

### 3.3. Self-pressurization phase

During self-pressurization, the system is closed and the cryogen pressure and temperature evolution assumes again successive quasi-equilibrium saturation states. The external heat load  $\mathcal{P}_{h.l.}$  results in an interfacial evaporation from liquid to vapor and a tank self-pressurization from  $p_1^{end}$  to  $p_{max}$ . In order to correctly represent the non-linearities of the fluid properties over this pressure range, the pressure increase is divided into  $N$  increments corresponding also to  $i = 1, N$  temperature increments  $\Delta T_{sp}^i = T_1^{i+1} - T_1^i$ . The thermodynamic balance equations previously introduced in the cooling phases are used again to derive the self-pressurization time  $t_{sp}^i$  of each pressure increment :

$$t_{sp}^i = \frac{1}{\mathcal{P}_{h.l.}} \left( m_{vap}^i \cdot \Delta(c_{vap} \cdot \Delta T_{sp}^i) + m_{liq}^i \cdot \Delta(c_{liq} \cdot \Delta T_{sp}^i) \right) + \frac{m_{vap}^i}{\mathcal{P}_{h.l.}} \times \left( \left(\frac{T_1^{i+1}}{T_1^i}\right)^{\frac{aM}{R}-1} \times \exp\left[\frac{bM}{R} \left(\frac{1}{T_1^i} - \frac{1}{T_1^{i+1}}\right)\right] - 1 \right) \times \left( (c_{vap}(T_1^{i+1}) - c_{liq}(T_1^{i+1}))T_1^{i+1} + L_{vap}(T_1^i) \right) \quad (5)$$

as well as the corresponding liquid mass evaporated  $\Delta m_{evap}^i$  :

$$\Delta m_{evap}^i = m_{vap}^i \times \left( \left(\frac{T_1^{i+1}}{T_1^i}\right)^{\frac{aM}{R}-1} \times \exp\left[\frac{bM}{R} \left(\frac{1}{T_1^i} - \frac{1}{T_1^{i+1}}\right)\right] - 1 \right) \quad (6)$$

The self-pressurization phase ends when the pressure in the tank reaches  $p_{max}$ . The cryogen masses are updated based on  $\Delta m_{evap}$  computed as  $\sum_{i=1}^N \Delta m_{evap}^i$ . If the liquid mass in the tank remains above the stopping threshold, a new cooling phase can be initiated.

### 3.4. Model validation

The homogenous thermodynamic model developed to describe the tank pressure and temperature evolution during a self-pressurization phase and a TVS regulation phase is validated using experimental data made available in the study (12). Various self-pressurization and TVS injection experiments are performed in (12) for a 110 L tank using as simulant fluid 3M<sup>TM</sup>NOVEC<sub>1230</sub>, a fluoroketone which vaporizes at 50°C under atmospheric pressure. This experimental study explores the influence of various control parameters (such as tank filling  $\mathcal{F}$ , tank heat load  $\mathcal{P}_{h.l.}$  and injection mass flow rate  $\dot{m}_{inj}$ ) on the temperature and pressure variation in the tank. The measured evolution of the averaged tank temperature  $T_{ave}$ , for a self-pressurization phase taking place with  $\mathcal{F} = 66\%$  and  $\mathcal{P}_{h.l.} = 26 W$ , is displayed in Fig.6 along with the temperature  $T_{mod}$  predicted by the homogeneous thermodynamic model. The agreement between measurement and model prediction can be considered as satisfactory with a difference on the self-pressurization time (defined in the present case as the time needed to reach a 5 K increase for the tank temperature) below 1%. The TVS injection experiment is performed for the same choice of  $\mathcal{F}$  and  $\mathcal{P}_{h.l.}$  with an injection mass flow rate set equal to  $\dot{m}_{inj} = 43 g.s^{-1}$ . The final plateau temperature is well captured by the model with an error below 0.2% with respect to the experiment. The exponential temperature decrease, induced by the sub-cooled injection, is correctly reproduced, even though the dynamic response of the model does not perfectly match the experimental behavior. It was also checked on these reference experiments that the choice  $\Delta\tau = 5 s$  for the timestep and  $N=15$  for the number of pressure increments in the self-pressurization stage was sufficient to ensure a converged numerical prediction - a further refinement of the timestep or increase of the increments number does not longer modify the model prediction.

## 4. Regulation history of an arbitrarily designed TVS system

The range of variation for each of the 12 input parameters describing the TVS regulation system is reported in Table 4. An *a priori* selection of these design parameters defines an arbitrary TVS system (see Table 4), the performance of which is now assessed using the numerical model described in the previous section for the tank thermodynamic states and in Appendix A for the remainder of the TVS system components; the system performance is eventually compared to the reference ideal DV system. The pressure history predicted

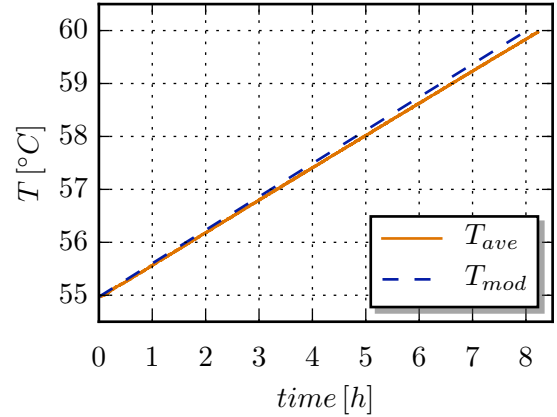


Figure 6: Experimental ( $T_{ave}$ ) and model ( $T_{mod}$ ) temperature history during a self-pressurization experiment (12) for the following control parameters value :  $\mathcal{F} = 66\%$  and  $\mathcal{P}_{h.l.} = 26 W$ .

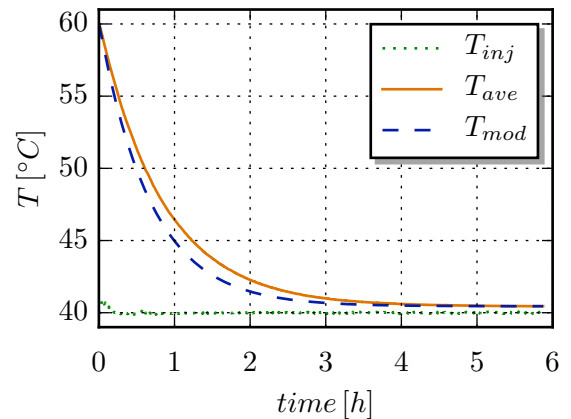


Figure 7: Experimental ( $T_{ave}$  and  $T_{inj}$ ) and model ( $T_{mod}$ ) temperature history during a TVS injection experiment (12) for the following control parameters value :  $\mathcal{F} = 66\%$ ,  $\mathcal{P}_{h.l.} = 26 W$  and  $\dot{m}_{inj} = 43 g.s^{-1}$ .

by the model during the whole TVS regulation is displayed in Fig.8. The tank pressure  $p_1$  decreases during the cooling phases until a minimum value is reached. Furthermore the maximum pressure reached at the end of each self-pressurization phase decreases from one cycle to the next due to a non-zero value of  $\alpha_p$ . The cooling dynamics evolves over time : as the cryogen mass in the tank decreases over time (see Fig.11), the fluid inertia also significantly decreases which explains the predicted transient behavior. Furthermore one can observe that the flow through the venting branch experiences an isenthalpic expansion in the JT valve resulting in a pressure and temperature drop respectively down to  $p_2$  and  $T_2$  as can be observed in Fig.8 and Fig.9. The cooling

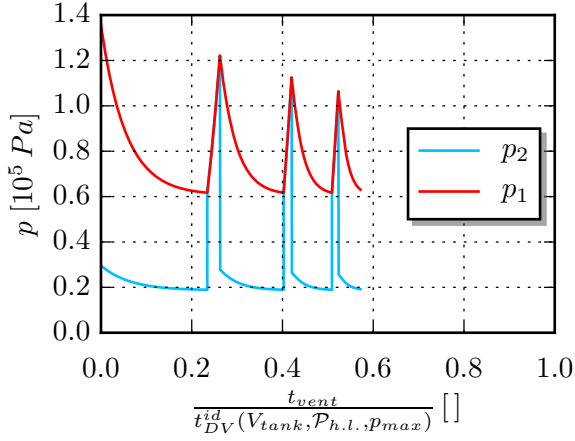


Figure 8: Pressure history for the different thermodynamic cycle point (see Fig.5) during an *a priori* designed TVS regulation.

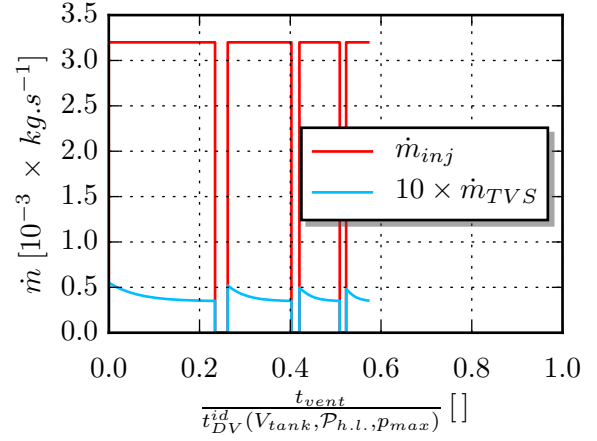


Figure 10: Mass flowrate history in the injection loop and the vented branch (see Fig.4) during an *a priori* designed TVS regulation.

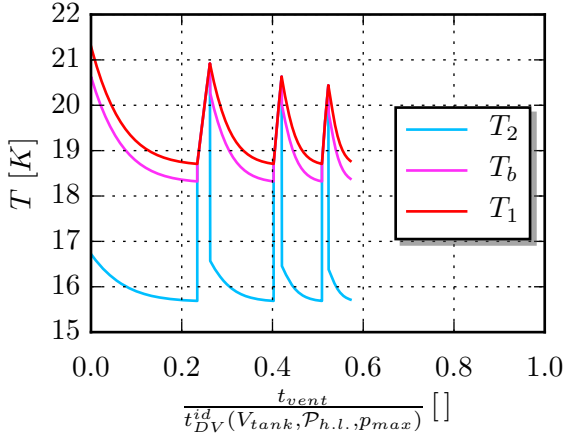


Figure 9: Temperature history for the different thermodynamic cycle point (see Fig.5) during an *a priori* designed TVS regulation.

power of this flow is transferred, thanks to the heat exchanger, to cool the injection loop down to the injection temperature  $T_b$ . The temperature difference between the tank ( $T_1$ ) and the sub-cooled jet ( $T_b$ ) slightly increases during a cooling phase. The subcooled injection, with a constant mass flow rate, induces tank pressure ( $p_1$ ) and temperature ( $T_1$ ) decrease.

During a self-pressurization phase, the injection pump is turned off, the vented branch is closed ( $\dot{m}_{inj} = \dot{m}_{TVS} = 0$  in Fig.10) and the tank pressure (and temperature) rises in the tank due to the external heat load ( $\mathcal{P}_{h.l.}$ ) and the internal interfacial heat and mass transfer until the maximum pressure is reached. Furthermore, one can notice in Fig.10 that the mass flow rate in the vented branch depends on the tank pressure. Indeed, as the tank

pressure decreases, the pressure gradient generating the flow in the vented branch also decreases which induces the computed mass flow rate reduction. Fig.11 displays the cryogen mass reduction over time due to fluid consumption through the vented branch during cooling phases. Note that during self-pressurization, the total mass remains constant while liquid mass is transferred to the vapor phase because of evaporation. The perfor-

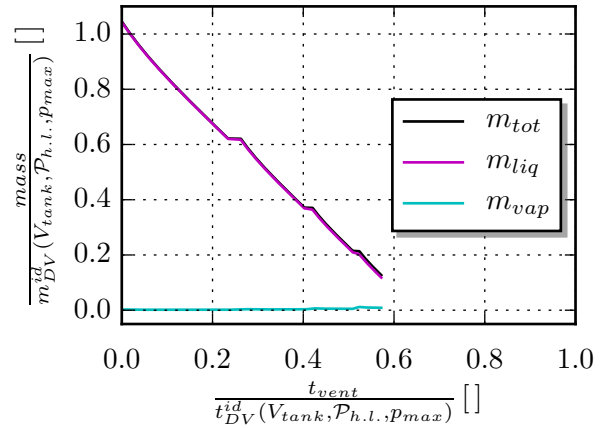


Figure 11: Cryogen mass history in the the tank during an arbitrarily designed TVS regulation.

mance characteristics of this arbitrarily designed TVS system are quite low when compared to an ideal DV system. Indeed, as indicated by all the previously analyzed time evolution plots, the venting time of the TVS system does not exceed 60% of the venting time yielded by an ideal DV. Naturally, TVS remains nonetheless of interest since it can operate in space conditions, contrarily to

Description of the TVS design parameters. The minimum, maximum and discretization step values are used in the optimization process. The design values for the so-called arbitrary design correspond to the *a priori* analysis performed in section 4 with results reported in Fig.8 to 11. The design values for the CPST optimum correspond to the selected optimal design reported in Fig.12.

<b>Param.</b> <i>unit</i>	$L_{plate}$ [ $10^{-3} m$ ]	$l_{plate}$ [ $10^{-3} m$ ]	$t_{plate}$ [ $10^{-3} m$ ]	$\beta_{plate}$ [ $10^{-3} m$ ]	$\alpha_{exch}$ [ ]	$R_{vent}$ [ $10^{-3} m$ ]
min. - max.	1.0 – 150.0	1.0 – 150.0	0.01 – 2.0	0.2 – 2.0	0 – 1	0.1 – 2.0
step	0.5	0.5	0.01	0.1	1	0.1
arbitrary design	12.5	111.5	0.47	1.7	0.261	0.5
CPST optimum	149.5	90.0	0.01	0.4	0.7215	0.4

<b>Param.</b> <i>unit</i>	$K_{JT}$ [ $10^{12} Pa.kg^{-1}.s$ ]	$p_{max}$ [ $10^5 Pa$ ]	$p_{min}$ [ $10^5 Pa$ ]	$\alpha_p$ [ ]	$\dot{m}_{inj}$ [ $10^{-3} kg.s^{-1}$ ]	$\alpha_{OH}$ [ ]
min. - max.	0.1 – 90.0	0.3 – 3.5	0.1 – 0.29	0 – 1	0.1 – 5.0	0 – 1
step	0.1	0.01	0.01	0.01	0.05	1
arbitrary design	34.0	1.32	0.18	0.55	3.2	1.0
CPST optimum	41.03	0.42	0.14	0.09	0.9	1.0

the ideal DV. However this also suggests there is much room for improvement of the TVS design, keeping in mind the targeted TVS venting time is actually the ideal DV venting time computed for the same tank volume, submitted to the same heat load and operating at  $p_{max}$ . Since the typical calculation time needed to obtain the complete TVS regulation history does not exceed a few seconds when using the extended thermodynamic homogeneous model, a numerical optimization loop can be set up to identify the choice of design parameters allowing to maximize the venting time of a heated storage tank regulated using TVS.

## 5. Optimization loop setup

Optimizing the TVS system requires to find the set(s) of 12 design parameters yielding an optimal performance level characterized in the first place by the largest possible venting time. This first objective to maximize is completed with a second objective corresponding to the minimization of the number of control cycles so as to preserve the reliability of the regulation. A constraint is also added to the problem definition : the number of plates for the heat exchanger should be no lower than 2. The optimization process takes into account the fact the TVS system is self-contained in the tank : the initial mass of available propellant is computed from the fixed tank volume with the volume of TVS components subtracted, hence with a varying size for the heat exchanger from one design to the other. The multi-parameter bi-objective constrained optimization problem is solved using the Nondominated Sorting

Genetic Algorithm (NSGA-II) initially proposed in (19) and such as implemented in the commercial optimizer ModeFrontier. The design space defined in Tab.4 is explored using a population of 100 designs, evolved during 50 generations by application of selection, crossover and mutation genetic operators. It is systematically checked the optimal Pareto set found by the algorithm displays no significant evolution over the last few generations and can therefore be considered as converged.

## 6. Analysis of the results

### 6.1. Optimized TVS system for the CPST mission

The first optimization is performed for the baseline configuration of the CPST mission, that is a tank of volume 137 L submitted to an external heat load  $\mathcal{P}_{h.l.} = 10 W$ . The feasible designs computed by the optimization algorithm are displayed in the objective space in Fig.12, with the optimal Pareto designs indicated by dark blue symbols. The venting time is normalized by the venting time of an ideal DV (pure vapor) operating at the same conditions. The computed Pareto front contains 4 optimal designs corresponding to a regulation involving 1 to 4 cycles. One can observe that the optimized TVS system provides a venting time equivalent to the one (theoretically) yielded by an ideal DV system. The key interest of TVS lies naturally in the fact this level of performance can be actually achieved in space conditions since the liquid extraction required for both the injection loop and the vented branch can be performed using a Liquid Acquisition Device (20). If only one cycle of regulation is allowed, the best TVS design

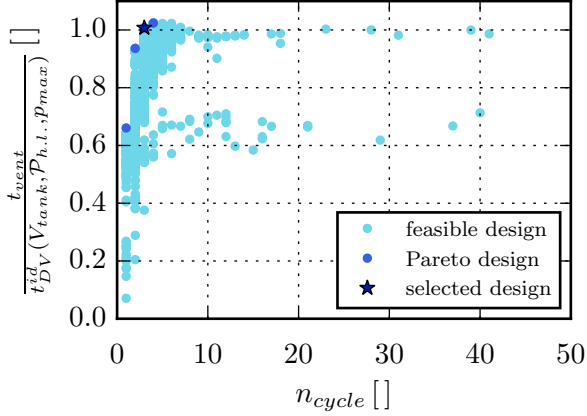


Figure 12: Results of the optimization procedure for the CPST tank mission. Representation of the feasible, the Pareto and the selected designs in the objective space.

provides only 60% of the ideal performance. The trade-off design indicated by the black star symbol in Fig.12 achieves 100% of the ideal venting time with only 3 regulation cycles. The corresponding design parameters are reported in Table 4.

The time evolution of the tank pressure  $p_1$  and the vented branch pressure  $p_2$  downstream the JT valve is displayed for this selected design in Fig.13. With pres-

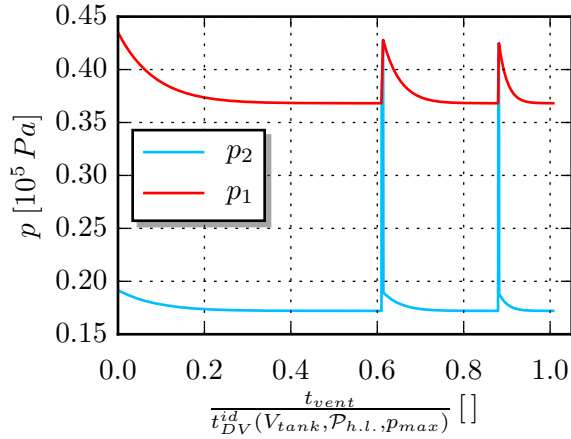


Figure 13: Pressure history for the different thermodynamic cycle points (see Fig.5) during the CPST optimized TVS system regulation.

sure levels remaining below  $0.45 \times 10^5 Pa$ , the computed optimal pressure regulation indicates a storage at low pressure is of interest to store cryogenes on a long term basis, at least for the heat load and tank volume under consideration. This low-pressure regulation permits to expel vapor with a lower enthalpy and thus maximizes

the cooling power of the vented branch. Note also the interest of the optimization loop is well demonstrated since a CPST design is found which increases the TVS performance with respect to the ideal DV from 60% to 100%. The design tool is next applied to the more general problem of finding optimal TVS designs for various tank sizes and heat loads.

## 6.2. Influence of tank volume on TVS performance

In order to assess the influence of tank volume on the system performance and on its (optimal) design, optimization runs have been performed with two larger tanks with respect to the small CPST tank. Fig.14 displays the converged Pareto fronts provided by NSGA-II for bi-objective constrained optimization processes corresponding to three different tank volumes ( $137 L$ ,  $1 m^3$ ,  $10 m^3$ ) with a fixed heat load  $\mathcal{P}_{h.l.} = 10 W$ . One can

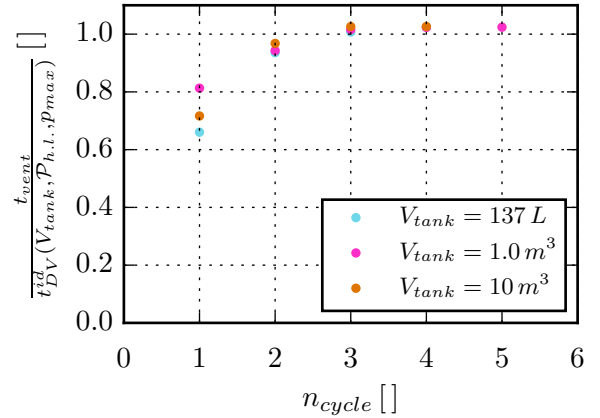


Figure 14: Pareto fronts of the optimization processes for tank heat load of 10 W and different tank volume.

observe that the tank volume has no noticeable effect on the performance achieved by the optimized TVS : the optimal values for the normalized venting time and pseudo-cycle number remain similar whatever the tank size. Furthermore, the similar Pareto fronts displayed in the objective space remain also similar when plotted in the 12-dimensional design space (not reported here for the sake of conciseness). Fig.15 shows the tank pressure history for the 3 investigated tank volumes regulated with the same optimal TVS system, namely the previously selected Pareto design for the CPST mission optimization. The regulation process is not, strictly speaking, the same when increasing the tank volume but remains nonetheless similar from one volume to the other, yielding the same normalized venting time equal to unity (that is an absolute TVS venting time equal to

100% of the corresponding ideal DV venting time) for the same number (3) of regulation pseudo-cycles. One can thus conclude that the tank volume impacts neither the optimal TVS system performance nor the optimal sizing of the system. It remains to investigate the impact of the prescribed heat load on the TVS design.

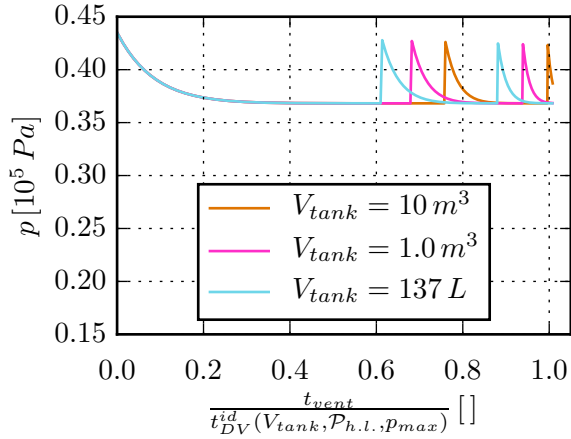


Figure 15: Tank pressure history obtained for different tank volumes submitted to a 10 W heat load and regulated with the same TVS system (previously selected design for the CPST mission optimization Fig.12).

### 6.3. Tank heat load influence on the TVS performances

As can be observed in Fig.16, the heat load influence on the Pareto front is strong : the optimal values of the pseudo-cycle number significantly vary with the tank heat load. However the maximum venting time of the optimized TVS systems remains always equivalent to the one yielded by an ideal DV system operating in analogous conditions. As the  $1\text{ m}^3$  tank heat load increases from 10 W to 100 W, the subcooled jet cooling power  $\mathcal{P}_{jet}$  (see Eq.1) increases as well to overcome evaporation effects induced by  $\mathcal{P}_{h.l.}$  and still ensures its cooling function. The TVS system can efficiently manage tank pressure only if its design ensures a ratio  $\frac{\mathcal{P}_{jet}}{\mathcal{P}_{h.l.}}$  above unity. The tank cooling dynamics is governed by this power ratio : the higher its value, the faster the cooling dynamics as shown in Fig.17 where the time-evolution of the jet cooling power is plotted for some selected Pareto designs taken from Fig.16. The selected designs are such they yield a normalized venting time above 0.96 and a minimum number of regulation pseudo-cycles. The jet cooling power can be modified by adjusting several design parameters : the injection mass flow rate, the dimensions of the heat exchanger, the venting throat radius, the pressure level in

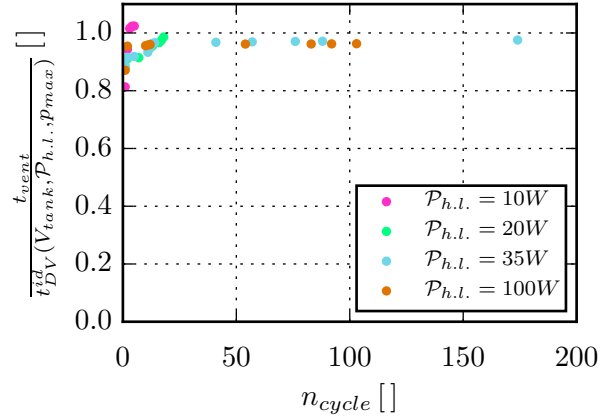


Figure 16: Computed Pareto fronts for the design optimization of a TVS applied to a tank of fixed volume ( $1\text{ m}^3$ ) submitted to various heat loads.

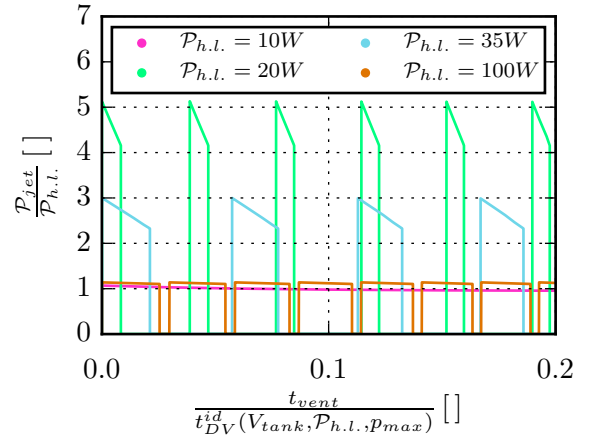


Figure 17: History of the thermal power ratio during the first 20% of some selected Pareto designs for various heat loads applied to a  $1\text{ m}^3$  tank.

the tank or a combination of these parameters. Fig.18 shows the tank pressure history corresponding to the optimal designs already analyzed in Fig.17. It shows that the optimal storage pressure level in the tank varies significantly with  $\mathcal{P}_{h.l.}$ . Indeed for a 10 W tank heat load  $p_{tank} \in [0.3 - 0.45] 10^5\text{ Pa}$  while for the other heat load values  $p_{tank} \in [0.9 - 1.5] 10^5\text{ Pa}$ . The observed storage pressure rise induces a mass flow rate increase in the vented branch yielding a subsequent increase for the subcooled jet cooling power. However the cross-dependency between the design parameters makes it difficult to identify a general rule or guideline for *a priori* designing an optimal TVS system whatever the tank heat load. The performed design process demonstrates

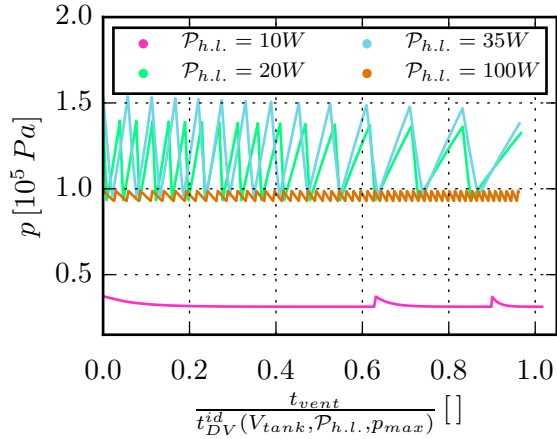


Figure 18: Tank pressure history under different tank heat load for the optimal design (*i.e.* design among the Pareto front yielding at least a normalized venting time of 0.96 with a minimum pseudo-cycle number).

however it is always possible, whatever the heat load (and tank volume), to find a TVS design yielding a venting time equivalent to the one of an ideal DV strategy.

## 7. Conclusion

Building on an efficient homogeneous thermodynamic model validated from on-ground experimental data, an optimization loop has been set up to perform the optimal design of a Thermodynamic Venting System for a  $LH_2$  storage tank of given size submitted to a prescribed heat load. The design tool has first been applied to a tank of 137 L submitted to a 10 W heat load, in the context of the future CPST demonstration mission. The optimized TVS system yields a performance level equivalent to the one of an ideal DV system venting pure vapor. Note this latter approach is only a theoretical reference as it would be technologically unfeasible in the context of space missions while TVS can be actually devised, using Liquid Acquisition Devices. Furthermore the influence of tank volume and heat load on the system performance has also been assessed using the same optimization tool. It is found that the tank volume impacts neither the TVS system performance (maximum achievable venting time) nor the system design parameters. As for the tank heat load variation, it does not impact the performance in the sense an optimized TVS system still yields a venting time equivalent to the corresponding ideal DV time. However the TVS design parameters vary significantly with the tank heat load. At this stage, no systematic guideline has been identified

which would allow an *a priori* prescription of the system design parameters for a given tank heat load.

Future work will be devoted to a further analysis of optimal designs to try to extract such guideline. This work might also be extended to include in the design process the minimization of the TVS system mass (as a function of the identified design parameters). Future optimization could also include into the storage history some realistic mission requirements regarding the propellant use, such as a number of engine restarts during a given mission time. It must be also reminded the tank model used in the present study does not account for gravity effects. It is therefore likely the homogeneous thermodynamic model will need to be tuned for 0g or low gravity applications, using high-fidelity CFD simulations since experimental data for TVS regulation in space conditions is not yet available. Note however that state-of-the-art CFD simulations of self-pressurization (or TVS) in cryogenics tanks are not yet fully predictive since relying on adjustable parameters (see for instance (14) or (21)). Moreover, a simplified homogeneous thermodynamic model such as the one used in the present study remains particularly attractive for optimal design because of its reduced computational cost.

## Acknowledgments

The authors acknowledge the joint support of the Centre National d'Etudes Spatiales (CNES) and Air Liquide Advanced Technologies (ALAT). The laboratory LEGI is part of the LabEx Tec 21 (Investissements d'Avenir - grant agreement n°ANR-11-LABX-0030)

## Appendix A. TVS components formulation

In this appendix, the balance equations used to model the behavior of the TVS system components, others than the storage tank itself, are described.

### Appendix A.1. Vented branch

In order to determine the actual vented branch working conditions, the vented mass flow rate  $\dot{m}_{TVS}$  and the pressure  $p_2$  are updated at each timestep during the cooling phase. These quantities depend on the tank pressure, the pressure drops in the JT-valve and the critical (sonic) condition imposed at the venting throat, as detailed hereafter.

### Appendix A.1.1. Joule-Thomson valve

The JT-valve creates an isenthalpic expansion of the fluid circulating in the vented branch (see transformation 1  $\rightarrow$  2 on Fig.5). This expansion is described through the fluid pressure drop  $\Delta P$  of the vented branch based on the mass flow rate  $\dot{m}_{TVS}$  and on the JT-valve pressure drop constant  $K_{JT}$  (characterizing the JT-valve geometry (17)) :

$$\Delta P = p_1 - p_2 = K_{JT} \cdot \dot{m}_{TVS}^2 \quad (\text{A.1})$$

### Appendix A.1.2. Venting throat

The venting throat ensures a critical (sonic) condition at the throat section. It permits to compute the vented branch mass flow rate as :

$$\dot{m}_{TVS} = S_{vent} \cdot p_i \left( \frac{\gamma}{rT_i} \right)^{1/2} \cdot \left( \frac{\gamma+1}{2} \right)^{-\frac{(\gamma+1)}{2(\gamma-1)}} \quad (\text{A.2})$$

$$S_{vent} = \pi \times R_{vent}^2$$

where  $T_i$  and  $p_i$  are respectively the fluid temperature and pressure conditions at the throat inlet,  $r = \frac{R}{M}$  is the hydrogen gaz constant and  $\gamma = \frac{C_p}{C_v}$  is the heat capacity ratio. Equation (A.2) relies on the classical hypothesis of vapor behaving as an ideal gas. The fluid inlet conditions (*i.e.*  $p_i$  and  $T_i$ ) vary during a cooling phase. However the relative pressure variation is much more important than the temperature variation :

$$\frac{p_{out}}{p_{in}} = \left( \frac{T_{out}}{T_{in}} \right)^{\frac{\gamma}{\gamma-1}}$$

Thus the inlet temperature  $T_i$  has no significant influence on the results and can be fixed to a constant value as follows :

$$T_i = \left( \frac{T_{sat}(p_{max}) + T_{sat}(p_{min})}{2} \right) \quad (\text{A.3})$$

Furthermore, the pressure drops downstream the JT-valve are neglected. Thus the throat inlet pressure  $p_i$  equals the thermodynamic cycle minimum pressure  $p_2$ .

### Appendix A.1.3. Vented branch flow conditions

During cooling phases, the vented branch flow conditions are derived at each timestep from Eq.A.1 and Eq.A.2, yielding :

$$\dot{m}_{TVS} = \left( \frac{p_1 - p_2}{K_{JT}} \right)^{1/2}$$

$$p_2 = \frac{\left( -1 + \left( 1 + 4 \cdot p_1 \cdot S_{vent}^2 \cdot K_{throat}^2 \cdot K_{JT} \right)^{1/2} \right)}{2 \cdot S_{vent}^2 \cdot K_{throat}^2 \cdot K_{JT}} \quad (\text{A.4})$$

$$K_{throat} = \left( \frac{\gamma}{rT_i} \right)^{1/2} \cdot \left( \frac{\gamma+1}{2} \right)^{-\frac{(\gamma+1)}{2(\gamma-1)}}$$

$$S_{vent} = \pi \times R_{vent}^2$$

### Appendix A.2. Injection loop

The main component of the injection loop is the heat exchanger. Prior to any regulation sequence, the heat exchanger size is determined based on the pressure limits of the considered regulation sequence. The injection pump power is calculated to overcome the pressure drops in the heat exchanger resulting in the subcooled jet injection. Then at each cooling phase timestep, the injection temperature is derived from the vented branch flow conditions. The heat exchanger size is initialized using the LMDT method while the injection temperature during cooling phases is updated using the NTU method.

#### Appendix A.2.1. Heat exchanger size initialization

The heat exchanger size is computed using the Logarithmic Mean Temperature Difference method (22). The two most constraining cases, corresponding respectively to  $p_1 = p_{max}$  and  $p_1 = p_1^{end}$  (*i.e.*  $p_2 = p_{min}$ ), are weighted by the numerical parameter  $\alpha_{exch}$  to obtain the final heat exchanger plate number  $n_{plate}$ .

The LMTD method calculates the exchange area  $S_{exch}$  necessary to transfer a given thermal power  $\mathcal{P}_{exch}$  :

$$\mathcal{P}_{exch} = K \cdot S_{exch} \cdot \Delta T_{LM} \quad (\text{A.5})$$

where  $K$  is the thermal transfer coefficient given by :

$$K = \left( \frac{1}{h_{TVS}} + \frac{t_{plate}}{\lambda_{plate}} + \frac{1}{h_{inj}} \right) \quad (\text{A.6})$$

with  $h_{TVS}$  and  $h_{inj}$  the convective heat transfer coefficient on both sides of the heat exchanger plates and  $\lambda_{plate}$  the plate thermal conductivity.  $\Delta T_{LM}$  is expressed as follows :

$$\Delta T_{LM} = \frac{(T_a - T_3) - (T_b - T_2)}{\log \left( \frac{T_a - T_3}{T_b - T_2} \right)} \quad (\text{A.7})$$

where  $T_b$  is estimated using the heat exchanger enthalpic balance :

$$\dot{m}_{inj} \cdot c_{p_{inj}} \cdot (T_a - T_b) = \dot{m}_{TVS} \cdot (h_3 - h_2) \quad (\text{A.8})$$

with  $c_{p_{inj}}$  the injected fluid heat capacity,  $T_a$  and  $T_b$  the tank and injection temperature and  $h_2$  and  $h_3$  the enthalpy values at states 2 and 3.

Assuming an adiabatic heat exchange, one obtains :

$$T_b = T_a - \frac{\dot{m}_{TVS} \cdot (h_3 - h_2)}{\dot{m}_{inj} \cdot c_{p_{inj}}} \quad (\text{A.9})$$

The heat exchange surface is thus simply computed along with the plate number :

$$S_{exch} = \frac{\dot{m}_{TVS} \cdot (h_3 - h_2)}{K \cdot \Delta T_{LM}} \quad (A.10)$$

$$\frac{S_{exch}}{L_{plate} \cdot l_{plate}} \leq n_{plate} \leq \left( \frac{S_{exch}}{L_{plate} \cdot l_{plate}} + 1 \right)$$

$$n_{plate} \in \mathbb{N}$$

Applying this method, to the two limiting cases corresponding respectively to  $p_{max}$  and  $p_{min}$ , the actual plate number is eventually computed as follows :

$$n_{plate}^* = \alpha_{exch} \cdot n_{plate}(p_{max}) + (1 - \alpha_{exch}) \cdot n_{plate}(p_1^{end})$$

$$n_{plate}^* \leq n_{plate} \leq (n_{plate}^* + 1)$$

$$n_{plate} \in \mathbb{N} \quad (A.11)$$

The heat exchanger plate number remains naturally fixed during the whole regulation sequence.

#### Appendix A.2.2. Injection Pump power calculation

The pump power required by the TVS system is calculated from the heat exchanger pressure drops (on the injection loop side). It is assumed here that the heat exchanger is composed of  $n_{plate}$  non-embossed plates. The pressure drops are derived considering the linear pressure drops which are then increased by 30% to take into account the restrictions and elbows effects :

$$\Delta P_{inj-loop} = (1 + 0.3) \cdot \left( \frac{\zeta \cdot L \cdot \rho \cdot v^2}{2 \cdot D_H} \right) \quad (A.12)$$

with  $\zeta$  the pressure drop coefficient,  $\rho$  the liquid density,  $L$  the fluid path length,  $v$  the flow speed, and  $D_H$  the hydraulic diameter. The pressure drop coefficient is simply estimated as :

$$\zeta = \frac{60}{Re} \text{ if } Re < 2300 \text{ and } \zeta = \frac{0.3164}{Re^{0.25}} \text{ if } Re > 400$$

with  $Re$  the Reynolds number based on  $v$ ,  $D_H$  and the fluid kinematic viscosity.

The pump power is then computed as follows :

$$\mathcal{P}_{pump} = \left( \frac{\dot{m}_{inj}}{\rho_{inj}} \cdot \Delta P_{inj-loop} \right) \cdot \frac{1}{\eta_{hyd}} \quad (A.13)$$

where  $\eta_{hyd}$  is the hydraulic efficiency which is fixed at  $\eta_{hyd} = 0.5$  for all the calculations, following the work of Bravais (18).

As the pump is embedded inside the tank, the pump dissipated thermal power  $\mathcal{P}_{pump}^{therm}$  is added to the external heat load  $\mathcal{P}_{h.l.}$  during the cooling phases (when the

pump is running) resulting in a corrected tank heat load  $\mathcal{P}_{h.l.}^*$  :

$$\mathcal{P}_{h.l.}^* = \mathcal{P}_{h.l.} + \mathcal{P}_{pump}^{therm} \quad (A.14)$$

$$\mathcal{P}_{pump}^{therm} = \mathcal{P}_{pump} \cdot (1 - \eta_{hyd})$$

#### Appendix A.2.3. Injection temperature derivation

The injection temperature is calculated at each cooling phase timestep based on the previously computed heat exchanger dimensions and the vented branch flow conditions, using an adaptation of Number of Transfer Unit method (NTU) for phase change heat exchanger :

$$NTU = \frac{K \cdot S_{exch}}{\dot{m}_{inj} \cdot c_{p_{inj}}} \quad (A.15)$$

with  $K$  the heat transfer coefficient given by Eq.(A.6). The thermal power exchanged can be expressed as :

$$\mathcal{P}_{exch NTU} = E \cdot \dot{m}_{inj} \cdot c_{p_{inj}} \cdot (T_a - T_2) \quad (A.16)$$

with  $E = 1 - e^{-NTU}$  the exchanger efficiency.

Equalizing this quantity with the jet cooling power given by Eq.1, a first formulation of the injection temperature - corresponding to a thermal exchange limiting case - can be derived :

$$T_{b_{exch}} = T_1 - \frac{\mathcal{P}_{exch NTU}}{\dot{m}_{inj} \cdot c_{p_{inj}}} \quad (A.17)$$

Another way of deriving the injection temperature is to use the heat exchanger enthalpic balance :

$$\begin{cases} \dot{m}_{inj} c_{p_{inj}} (T_a - T_b) = \dot{m}_{TVS} (h_3 - h_2) & \text{if } \alpha_{OH} = 0 \\ \dot{m}_{inj} c_{p_{inj}} (T_a - T_b) = \dot{m}_{TVS} (h_{3'} - h_2) & \text{if } \alpha_{OH} = 1 \end{cases} \quad (A.18)$$

with :

$$h_{3'} = h_3 + c_{p_{vap}} (T_{3'} - T_3)$$

$$= h_3^0 + c_{p_{vap}} ((T_1 - \Delta T_{overheat}) - T_3) \quad (A.19)$$

This formulation yields another injection temperature formulation - corresponding to an enthalpic balance limiting case - which reads :

$$\begin{cases} T_{b_{enth}} = T_1 - \frac{\dot{m}_{TVS} \cdot (h_3 - h_2)}{\dot{m}_{inj} \cdot c_{p_{inj}}} & \text{if } \alpha_{OH} = 0 \\ T_{b_{enthOH}} = T_1 - \frac{\dot{m}_{TVS} \cdot (h_{3'} - h_2)}{\dot{m}_{inj} \cdot c_{p_{inj}}} & \text{if } \alpha_{OH} = 1 \end{cases} \quad (A.20)$$

In addition, another constraint on the injection temperature calculation is given by thermal irreversibilities associated with thermal exchange. The parameter  $\Delta T_{min\ exch} = 0.2^\circ C$  (see Fig.5) is introduced in order to limit the injection temperature to physical values by prescribing :

$$T_{b_{irrev}} = T_2 + \Delta T_{min\ exch} \quad (A.21)$$

The injection temperature eventually calculated at each cooling phase timestep is chosen to be the most restrictive of the three above formulations :

$$T_b = \begin{cases} \max(T_{b_{exch}}, T_{b_{enth}}, T_{b_{irrev}}) & \text{if } \alpha_{OH} = 0 \\ \max(T_{b_{exch}}, T_{b_{enth_{OH}}}, T_{b_{irrev}}) & \text{if } \alpha_{OH} = 1 \end{cases} \quad (\text{A.22})$$

## References

- [1] R. B. Schweickart. Thermodynamic analysis of a demonstration concept for the long-duration storage and transfer of cryogenic propellants. *Cryogenics*, 64:283–288, 2014.
- [2] A. Majumdar, J. Valenzuela, A. LeClair, and J. Moder. Numerical modeling of self-pressurization and pressure control by a thermodynamic vent system in a cryogenic tank. *Cryogenics*, 74:113–122, 2016.
- [3] Charles H. Panzarella and Mohammad Kassemi. On the validity of purely thermodynamic descriptions of two-phase cryogenic fluid storage. *Journal of Fluid Mechanics*, 484:41–68, 2003.
- [4] C.S. Lin, Van Dresar N.T., and M.M. Hasan. A pressure control analysis of cryogenic storage systems. Technical report, NASA Technical Memorandum TM-104409, AIAA-91-2405, 1991.
- [5] D Bentz. Tank pressure by jet mixing control in low gravity. Technical Report March, NASA Contractor Report 191012, 1993.
- [6] L Hastings. An overview of NASA efforts on zero boiloff storage of cryogenic propellants. *Cryogenics*, 41(11-12):833–839, 2001.
- [7] C Panzarella, D Plachta, and M Kassemi. Pressure control of large cryogenic tanks in microgravity. *Cryogenics*, 44(6-8):475–483, 2004.
- [8] Stephen Barsi. *Ventless pressure control of cryogenic storage tanks*. PhD thesis, Case Western Reserve University, 2011.
- [9] Stephen Barsi and Mohammad Kassemi. Investigation of Tank Pressurization and Pressure Control-Part I: Experimental Study. *Journal of Thermal Science and Engineering Applications*, 5(4):041005, 2013.
- [10] Stephen Barsi and Mohammad Kassemi. Investigation of Tank Pressurization and Pressure Control-Part II: Numerical Modeling. *Journal of Thermal Science and Engineering Applications*, 5(4):041006, 2013.
- [11] L. Demeure. *Comportement thermodynamique de réservoirs d’ergols cryogéniques*. PhD thesis, Université de Grenoble, Grenoble, 2013.
- [12] S. Mer, J-P. Thibault, and C. Corre. Active Insulation Technique Applied to the Experimental Analysis of a Thermodynamic Control System for Cryogenic Propellant Storage. *Journal of Thermal Science and Engineering Applications*, 8(2):021024, 2016.
- [13] J-P. Thibault, C. Corre, L. Demeure, and S. Mer. Thermodynamic Control Systems for Cryogenic Propellant Storage During Long Missions. In *ASME 2014 4th Joint US-European Fluids Engineering Division Summer Meeting FEDSM2014*, pages 1–8, 2014.
- [14] M. Kassemi and O. Kartuzova. Effect of interfacial turbulence and accommodation coefficient on CFD predictions of pressurization and pressure control in cryogenic storage tank. *Cryogenics*, 2015.
- [15] M.L Meyer, S. M. Motil, T. F. Kortes, and W. J. Taylor. Cryogenic Propellant Storage & Transfer (CPST) Technology Demonstration for Long Duration In-Space Missions. Technical report, NASA, Bordeaux, 2012.
- [16] M. L. Meyer, M. P. Doherty, and J. P. Moder. Technology Maturation in Preparation for the Cryogenic Propellant Storage and Transfer (CPST) Technology Demonstration Mission (TDM). Technical report, NASA GRC-E-DAA-TN14844,E-18896, 2014.
- [17] S Papell, T E D Nyland, and Naseem Saiyed. Liquid hydrogen mass flow through a multiple orifice Joule-Thomson device. *27th Thermophysics Conference*, 1992.
- [18] P. Bravais, F. Durand, and J. Lacapere. Pre-etude d’une pompe de transfert cryogénique pour l’alimentation d’un ”spray-bar”. Technical report, Air Liquid Advanced Technology - WP CTE3, Grenoble, 2006.
- [19] Kalyanmoy Deb, Amrit Pratap, Sameer Agarwal, and T. Meyarivan. A fast and elitist multiobjective genetic algorithm: NSGA-II. *IEEE Transactions on Evolutionary Computation*, 6(2):182–197, 2002.
- [20] J W Hartwig, D J Chato, J B McQuillen, J Vera, M T Kudlac, and F D Quinn. Screen channel liquid acquisition device outflow tests in liquid hydrogen. *Cryogenics*, 64:295–306, 2014.
- [21] Juan Fu, Bengt Sundén, Xiaoqian Chen, and Yiyong Huang. Influence of phase change on self-pressurization in cryogenic tanks under microgravity. *Applied Thermal Engineering*, 87:225–233, 2015.
- [22] J.M. Kay and R.M. Nedderman. *Fluid Mechanics and Transfer Processes*. Cambridge University Press, 1985.